The Astrophysical Journal Letters, 787:L10 (5pp), 2014 May 20 doi:10.1088/2041-8205/787/1/L10

DISCOVERY OF FINELY STRUCTURED DYNAMIC SOLAR CORONA OBSERVED IN THE Hi-C TELESCOPE

Amy R. Winebarger[1], Jonathan Cirtain[1], Leon Golub[2], Edward DeLuca[2],
Sabrina Savage[1], Caroline Alexander[1], and Timothy Schuler[3]
[1] NASA Marshall Space Flight Center, ZP 13, Huntsville, AL 35812, USA; amy.r.winebarger@nasa.gov
[2] Harvard-Smithsonian Center for Astrophysics, 60 Garden Street, Cambridge, MA 02138, USA
[3] State University of New York College at Buffalo, 1300 Elmwood Avenue, Buffalo, NY 14222, USA
Received 2014 January 31; accepted 2014 April 16; published 2014 May 2

ABSTRACT

In the Summer of 2012, the High-resolution Coronal Imager (Hi-C) flew on board a NASA sounding rocket and collected the highest spatial resolution images ever obtained of the solar corona. One of the goals of the Hi-C flight was to characterize the substructure of the solar corona. We therefore examine how the intensity scales from AIA resolution to Hi-C resolution. For each low-resolution pixel, we calculate the standard deviation in the contributing high-resolution pixel intensities and compare that to the expected standard deviation calculated from the noise. If these numbers are approximately equal, the corona can be assumed to be smoothly varying, i.e., have no evidence of substructure in the Hi-C image to within Hi-C's ability to measure it given its throughput and readout noise. A standard deviation much larger than the noise value indicates the presence of substructure. We calculate these values for each low-resolution pixel for each frame of the Hi-C data. On average, 70% of the pixels in each Hi-C image show no evidence of substructure. The locations where substructure is prevalent is in the moss regions and in regions of sheared magnetic field. We also find that the level of substructure varies significantly over the roughly 160 s of the Hi-C data analyzed here. This result indicates that the finely structured corona is concentrated in regions of heating and is highly time dependent.

Key word: Sun: corona

1. INTRODUCTION

A primary goal of the High-resolution Coronal Imager (Hi-C) was to observe and characterize the coronal structure. Several recent studies have compared the properties of structures observed with Hi-C to the structures observed with the lower-resolution Atmospheric Imaging Array (AIA) on the *Solar Dynamics Observatory* (*SDO*; see, for instance, Cirtain et al. 2013; Morton & McLaughlin 2013; Testa et al. 2013; Winebarger et al. 2013; Peter et al. 2013; Brooks et al. 2013; Alexander et al. 2013; Régnier et al. 2014). Two of these studies specifically focus on comparing the widths of linear structures, or coronal loops, in Hi-C and AIA data. Brooks et al. (2013) measured the width of 91 loop segments observed with Hi-C and found the most frequent Gaussian width of the Hi-C structures was 270 km, which is below the resolution of AIA. Additionally, they found several examples where Hi-C resolves multiple linear structures in what appears to be a single loop observed with AIA. There were also several examples where both Hi-C and AIA appear to observe the same monolithic structure, i.e., the loop either had no substructure or it was below the resolving power of Hi-C. In Peter et al. (2013), they calculate that if these loops are structured below what Hi-C can resolve, the diameters for the composite strands would have to be less than 15 km.

These papers relied on comparing the intensity profiles across the width of the structures observed in both AIA and Hi-C. However, evidence of substructure can also be found by comparing the intensity in low-resolution pixels to the distribution of intensities found in the high-resolution pixels. If the corona is smoothly varying, then all the photons hitting a single low-resolution pixel would be smoothly distributed among the high-resolution pixels within the limits of the noise of the observations. If the corona is structured at small spatial scales, then the intensity would not be distributed evenly in the high-resolution pixels. Instead, some of the pixels would be brighter than the uniform distribution, some would be dimmer. The width of the distribution of intensities of the high-resolution pixels provides indication of the level of substructure.

In this Letter, we present analysis of images of Active Region 11520 observed with Hi-C, which obtained high spatial and temporal resolution images of the solar corona during a sounding rocket flight. The goal of this Letter is to compare how the intensity distribution scales from high-resolution to low-resolution images. For ease of comparison, we degrade the Hi-C data to the AIA resolution and generate images with the same throughput, effective area, and cadence of the original Hi-C data. For each low-resolution pixel, we calculate the standard deviation in the high-resolution intensities that contribute to the pixel and compare it to the expected standard deviation calculated from the noise. If the ratio of these two numbers is $\sim$1, it indicates that the corona is varying smoothly and has no substructure, at least to the limit that Hi-C can positively detect it, given its noise levels. If the ratio is larger than 1, it indicates the presence of substructure. We find fine structure, located primarily in the moss and regions of sheared field, is highly variable in time.

2. DATA AND ANALYSIS

Hi-C is a Ritchey–Chretien telescope with a 220 mm diameter primary mirror and an effective focal length of 23.9 m. The primary and secondary mirrors have a multilayer coating that reflects a narrow wavelength window around 193 Å. The effective area of Hi-C is similar in wavelength response to that of the AIA 193 Å channel, though it is 5.3 times larger. Images are projected onto a 4096×4096 back-illuminated CCD. The plate scale of the images is $0\farcs103$ pixel^{-1}; the field-of-view of the telescope is $6\farcm8 \times 6\farcm8$. The payload was launched at approximately 18:50 UT 2012 July 11 from White Sands Missile Range. Hi-C acquired 37 full-frame images with a 2 s exposure time (5.5 s cadence). The resolution of the images is a result of the point-spread function of the optics and the stability of the

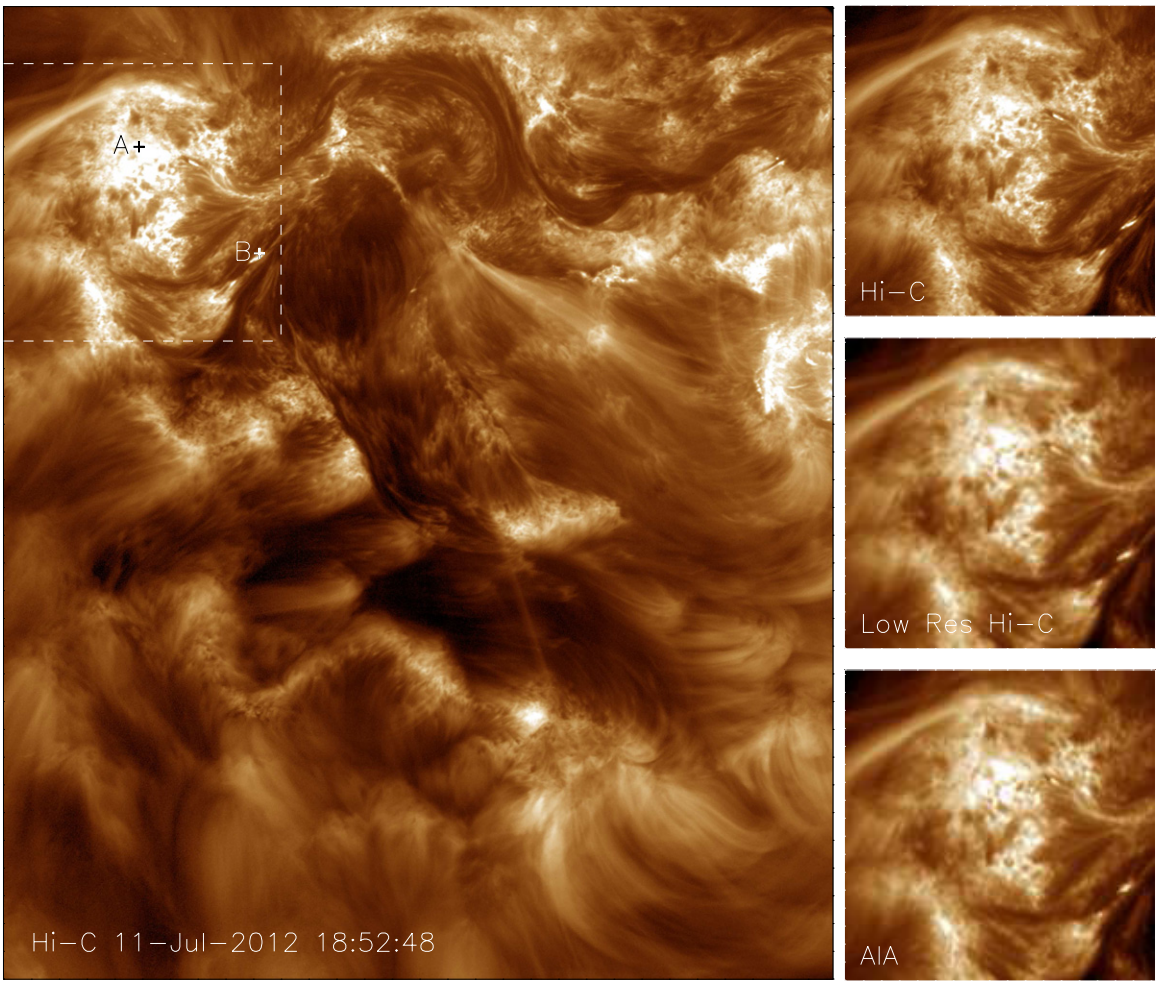

Figure 1. Left panel: the Hi-C 193 Å field of view considered in this analysis. The location of two example points, shown in Figure 2, are marked with plus signs. A subset of this region is shown in the three panels on the right. The top panel is the original Hi-C data, the middle panel is the low-resolution Hi-C data, and the bottom panel is the AIA data closest in time to the Hi-C data.

pointing control. The initial seven frames were blurred due to rocket jitter. One additional image was blurred due to a pointing maneuver approximately 2.5 minutes after the start of data acquisition. We estimate that the remaining 29 images have a resolution of 0.3–0.″4.

In this analysis, we only consider the full-frame, full-resolution images and we remove from the data set several images for which the sounding rocket pointing was not stable, so that the image quality was degraded. We remove the first seven images from the data set and we replace one image blurred by a re-pointing maneuver with the average of the images taken before and after the blurred image to maintain the cadence of the observations. The result is 30 Hi-C images with 5.5 s cadence. The Hi-C data were dark-current subtracted and flatfielded to remove the shadow of the filter mesh on the image. Dust was present on the Hi-C detector. Pixels that were effected by dust are corrected by interpolating from the nearest neighbor pixels not effected by dust. The images are co-aligned to correct for pointing drift and jitter of the rocket. Finally, the images are also corrected for atmospheric absorption by normalizing each image to the maximum of the total intensity summed over the image. Additional information on the Hi-C telescope, rocket flight, and data processing can be found in Kobayashi et al. (2013).

The target of the Hi-C flight was Active Region 11520 centered at approximately [−150, −281] arcsec from the center of the Sun. Figure 1 shows the region of the Hi-C field of view that is considered in this analysis.

The AIA (Lemen et al. 2012) flown on the *SDO* recorded full-disk solar images during the Hi-C rocket flight. In this analysis, we only examine the AIA 193 Å channel; images in this channel were taken with a cadence of 12 s, about a factor of 2 larger than the cadence of Hi-C. The pixel size of the AIA instrument is 0.″6 pixel^{-1}; it has a spatial resolution of ∼1.″2. The AIA data were aligned to the Hi-C data by cross-correlating the AIA 193 Å image to the Hi-C 193 Å images. The AIA data was rotated 1.°8 to correct for a small roll of the Hi-C telescope. We use the 15 co-aligned AIA images that were taken closest in time to the 30 Hi-C images.

There are some difficulties comparing the AIA and Hi-C intensities directly, namely that the telescopes have different throughputs (Hi-C has roughly 5.3 times the effective area of AIA) and the shape of the effective area curve is quite different at wavelengths away from the peak. Hi-C used improved multilayer coatings that suppressed the wavelength range of 180–185 Å significantly when compared to AIA. Additionally, there may be problems with alignment between the data sets and the images are offset in time. Therefore, we generate a low-resolution, "AIA-like" Hi-C data set. We first smooth the Hi-C data with a boxcar function with a width of 12 Hi-C pixels (roughly 2 AIA pixels) and then re-bin the data to AIA pixel size. The right panels in Figure 1 compare the Hi-C, low-resolution

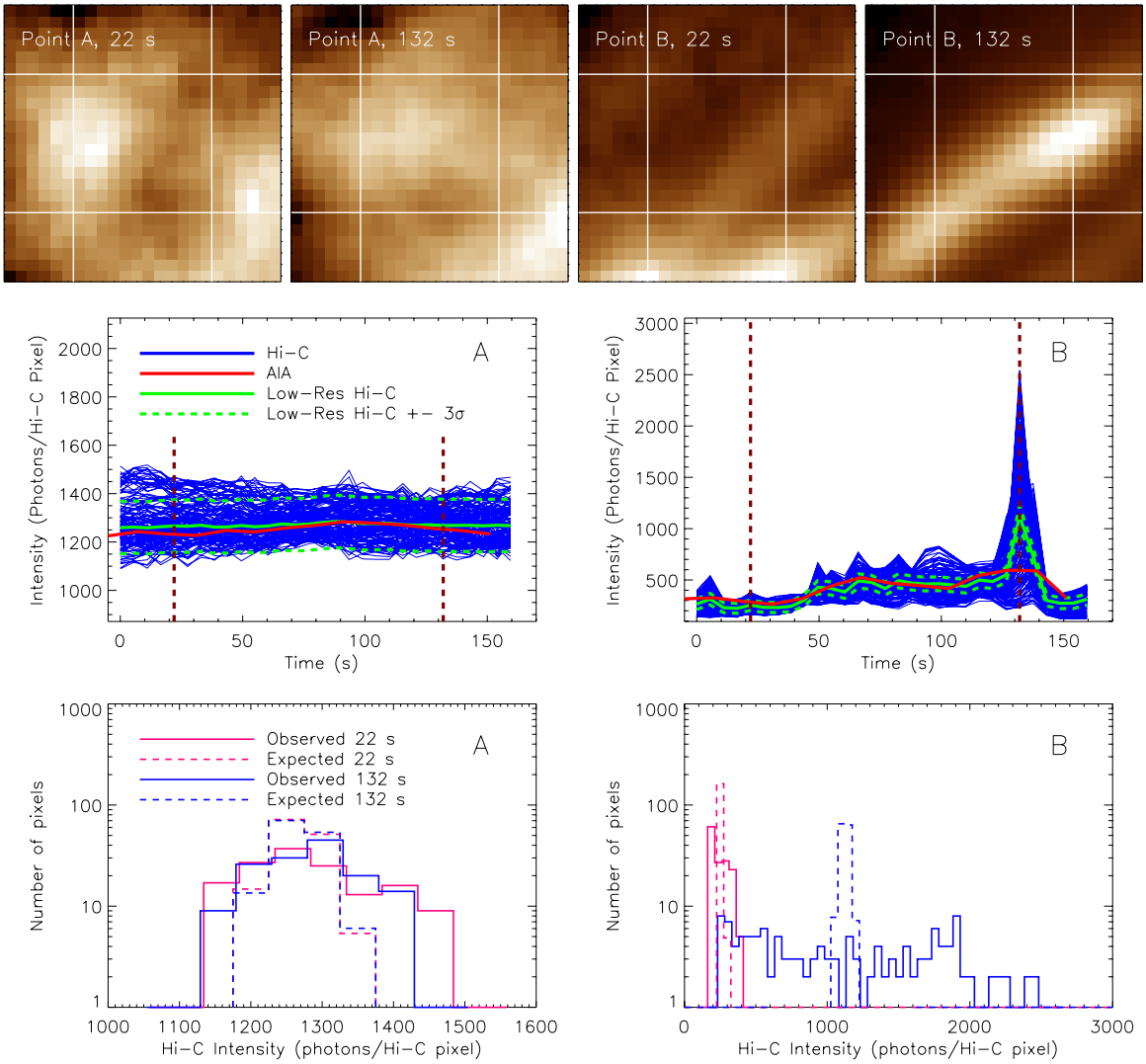

Figure 2. Top panels: Hi-C images around Point A and Point B shown in Figure 1 shown at two times in the Hi-C image sequence. The solid white lines show the boundaries of the 12×12 HI-C pixel that contribute to single low-resolution pixels. Middle panels: light curves of 144 Hi-C pixels (blue) that contribute to the single, low-resolution light curve (green). The red lines shown the co-spatial intensity in the AIA data. Green dashed lines show the low-resolution intensity $\pm 3\sigma$. The vertical dashed lines show the two times where we examine the distribution of intensities. Bottom panels: histograms of the 144 Hi-C intensities that contribute to a single low-resolution intensity. The distribution of intensities from 22 s is shown in red and 132 s is shown in blue. The expected Gaussian distributions associated with noise in the data are shown with dashed lines.

Hi-C and AIA images. Visual inspection reveals that these low-resolution data appear very similar to the actual AIA data, but they have the benefit of being (1) perfectly aligned to Hi-C, (2) perfectly in sync with Hi-C, with an image for every Hi-C image instead of roughly every other Hi-C image, and (3) have the identical throughput to Hi-C.

The goal of this analysis is to understand how the distribution of emission varies from low-resolution to high-resolution pixels. We investigate this behavior by comparing the intensity in a single pixel of the low-resolution Hi-C data to the 144 (12×12 Hi-C pixel) intensities that contributed to that low-resolution (smoothed and binned) intensity. The top panels of Figure 2 show subregions of the Hi-C field of view from the points labeled A and B in Figure 1. The center square of these images show 12×12 Hi-C pixels; these pixels contribute to a single low-resolution intensity. Point A is taken in the moss, point B is taken in an region of a loop brightening. The middle panels of Figure 2 show lightcurves of these pixels. The band of blue lines shows the 144 individual Hi-C light curves that contribute to the single low-resolution light curve. The low-resolution light curve, shown with the green line, is corrected for the difference between the high-resolution and low-resolution pixel size. The red line is the AIA light curve, which has been corrected for both the difference in throughput and pixel size. Note that the AIA light curves and low-resolution Hi-C light curves closely match one another. For simplicity, we will only compare the Hi-C intensities to the low-resolution Hi-C intensities and no longer include AIA.

If the solar corona varies smoothly, i.e., there is no substructure in the low-resolution pixel, then the high-resolution pixel intensities would form a Gaussian distribution around the low-resolution intensity, with the width of the Gaussian related to the expected noise. We assume that the noise in the data is due to the photon noise and the readout noise of the instrument and ignore any additional sources of noise, i.e., $\sigma = \sqrt{I_{\rm LR} + \sigma^2_{\rm readout}}$, where $I_{\rm LR}$ is the low-resolution intensity in photons per high-resolution pixel and $\sigma_{\rm readout}$ is the readout noise converted to photons. The readout noise of Hi-C has been found from analysis of the dark frames and varies by quadrant, with the least noisy quadrant having 16.0 DN (rms) and the noisiest quadrant 36.4 DN. The gain of the Hi-C detector is 4.3 e^- DN^{-1}. In

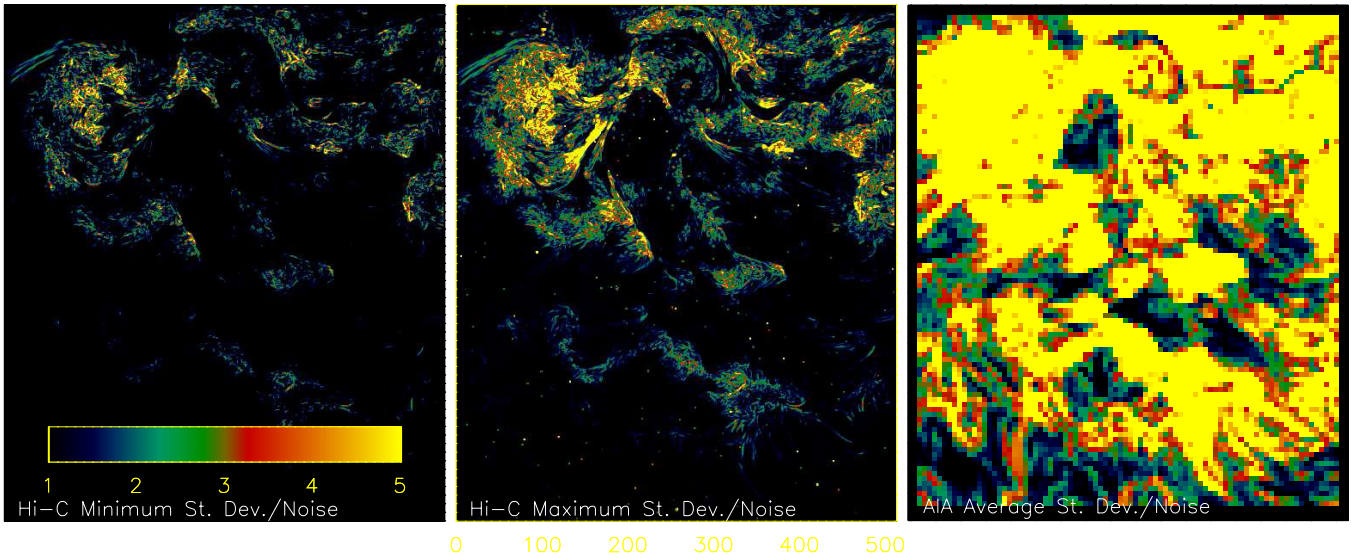

Figure 3. Minimum (left panel) and maximum (middle panel) of the ratio of the standard deviation in the Hi-C intensities to the noise. The average ratio of the standard deviation to noise for the AIA data is shown in the right panel.

Table 1
Calculated Standard Deviations Compared to Noise

Point	Time	St. Dev.	Noise	St. Dev./Noise
A	22 s	84.6	36.1	2.3
A	132 s	66.8	36.1	1.9
B	22 s	60.5	17.0	3.6
B	132 s	654.6	34.1	19.2

Table 2
Percentage of Pixels with Given Ratios

	Hi-C Minimum St. Dev./Noise	Hi-C Maximum St. Dev./Noise	AIA Minimum St. Dev./Noise	AIA Maximum St. Dev./Noise
$\leqslant 1$	81.3	53.7	3.9	0.6
1–3	17.2	40.3	32.0	28.2
3–5	1.3	4.7	22.6	23.7
>5	0.2	1.3	41.4	47.4

the 193 Å passband, there are approximately 17.6 e^- generated from each incoming photon. These numbers imply the readout noise is $\sigma_{\rm readout} = 3.9$ photons in the least noisy quadrant and $\sigma_{\rm readout} = 8.9$ photons in the noisiest quadrant. In the upper left quadrant, the location of both example pixels, the readout noise is 24.4 DN or 6.0 photons. At each time in the light curve, the expected noise is calculated. The dashed green lines in Figure 2 show the low-resolution intensity $\pm 3\sigma$.

The intensities around Point A do not change significantly over the 160 s, either in the low-resolution or high-resolution Hi-C data shown here. The intensity in the high-resolution, Hi-C pixels, shown in blue, are generally within the $\pm 3\sigma$ lines, shown as dashed green, though there are a few light curves above and below these values. Light curve B shows a short, transient brightening. During the entire light curve, the spread in the Hi-C intensities is larger than $\pm 3\sigma$ of the low-resolution value. At the peak of the brightening, this spread is particularly pronounced. Some of the Hi-C pixels are involved in the event, while others are not and stay at background levels throughout the event.

This is further demonstrated in the histograms shown in the lower panels of Figure 2. These histograms correspond to the two times shown in the upper panels and marked with vertical dashed lines in the middle panels of Figure 2. The observed histograms are shown with solid lines; the red line shows the histogram at 22 s and the blue line shows the histogram at 132 s. In addition, we show the expected distribution of intensities, meaning a Gaussian distribution centered around the low-resolution intensity with a standard deviation equal to the calculated noise, with dashed lines. For point A, there is very little change in the observed and expected distributions at the two times shown here. The observed histograms are broader than the expected histograms. The standard deviation in the 144 Hi-C intensities is given in Table 1 for both times; the standard deviations in the observed data is about twice the expected value calculated from the noise. In light curve B, the intensity distributions change dramatically between 22 s and 132 s. At neither time do the distributions resemble the expected Gaussian distribution, though the difference is most pronounced at the later time. The ratio of the calculated standard deviation in the data points to the noise, given in Table 1, is 3.6 at 22 s and 19.2 at 132 s.

Based on the above examples, we use the ratio of the standard deviation of the Hi-C intensities in a 12×12 pixel area to the expected noise calculated from the low-resolution intensity and readout noise as an indicator of substructure. Ratios close to 1 indicate that the distribution of Hi-C intensities in that 12×12 region can be explained by the photon and readout noise. Larger ratios indicate nonuniformity in the pixel intensities and suggest substructure.

For every pixel in the low-resolution data, for each frame of the Hi-C data, we calculate the standard deviation in the 144 Hi-C intensities that contribute to a single low-resolution intensity value and compare it to the expected noise. We find that, on average, 70% of the pixels in the Hi-C field of view have ratios <1, meaning the distribution of Hi-C intensities is consistent with noise levels. In Figure 3, we show the minimum value of this ratio in the 30 frames in the left panel and the maximum value of this ratio in the right panel. We further give the percentage of pixels in different ratio ranges in Table 2. In the minimum ratio image, 81% of the pixels in this image have a ratio of less than or equal to 1; in the maximum standard deviation image, 53.7% of the pixels fall into this category. In the

minimum ratio image, 17.2% of the pixels have ratios between 1 and 3. These pixels may be similar to the pixel A shown in Figure 2. We find that the ratio of the standard deviation to the noise can vary significantly over time in some pixels, like light curve B in Figure 2. Of the pixels that have a minimum ratio greater than 1, 52% show an increase in the ratio by at least 50%, and 13% of the pixels have an increase in the ratio by a factor of two in the 30 frames analyzed here.

Finally, for comparison, we complete identical analysis of the AIA data to determine if the results found above are typical of any similar change in resolution. We smooth the AIA data to 7.″2 resolution (the same jump in resolution as Hi-C to AIA) and bin it. We calculate the standard deviation in each 12×12 pixel area and compare it to the expected noise based on photon and readout noise. The average ratio calculated from the AIA data is shown in the right panel Figure 3. We also provide the percentage of these pixels with ratios in different range in Table 2.

The results for the AIA data are dramatically different from the Hi-C results. First, roughly 50% of pixels have ratios >5, indicating significant substructure. In addition, the ratios are more stable than in the Hi-C data. Only 3.5% of the pixels with ratio greater than 1 increase by 50% (compared to 52% in Hi-C), while only 0.9% of the pixels increase in ratio by a factor of two (compared to 13% in Hi-C).

3. DISCUSSION

In this Letter, we have analyzed the Hi-C data to determine if Hi-C is resolving structures previously unresolved by AIA. For ease of comparison, we degrade the Hi-C data to the AIA resolution and generate images with the same throughput, effective area, and cadence of the original Hi-C data. We demonstrate that the low-resolution Hi-C data visually resembles the AIA data and evolves similarly. We compare the distribution of the intensities of the 144 Hi-C pixels that contribute to a single, low-resolution pixel, to the expected distribution for a smoothly varying corona, meaning a Gaussian distribution with the width derived from the photon and readout noise. We show two example pixels, one where the contributing intensities are all relatively constant in time and have a slightly larger standard deviation than expected, and one where the contributing intensities vary significantly in time and deviate from the expected distribution significantly. We use the ratio of the standard deviation in the 144 contributing intensities to the expected noise as a marker for the presence of substructure. We find that the Hi-C intensity distributions in about 70% of the Hi-C field of view can be explained by noise. In the regions that cannot be explained by noise, namely the moss and regions of strong magnetic shear, we find the substructure varies significantly in time in the Hi-C data. For comparison, we completed identical analysis of the AIA data in the same region and found significantly different results, meaning the AIA data, when compared to 7.″2 resolution data, shows signs of substructure nearly everywhere. This substructure is approximately constant in time.

With Hi-C data, we identify regions that have no evidence of unambiguous substructure. This result implies that structures in these regions could be resolved by AIA; similar examples of structures that appear identical in Hi-C and AIA have been discussed by Brooks et al. (2013) and Peter et al. (2013). This analysis is, of course, limited by the throughput and readout noise of the Hi-C instrument. An instrument with the same resolution, but larger throughput (meaning more photons and less photon noise) and lower readout noise may be able to detect additional regions where the distribution of intensities cannot be explained by the noise.

The regions where there is evidence of substructure are typically in the moss and in areas of sheared field. The level of substructure in these regions can vary significantly with time, such as the example shown in Figure 2. The moss and sheared field area are regions of the strongest heating. These results indicate that heating is on smaller spatial scales than AIA and could be sporadic.

In this Letter, we have used the ratio of the standard deviation of Hi-C intensities to the noise as a method to identify regions of substructure. We have not used this measure to indicate the type of substructure (for instance, linear). Various combinations of substructure (a single linear structure, multiple linear structures, structures that are not linear) can create similar standard deviations. Calculating the standard deviation associated with different types of substructure is beyond the scope of this analysis and will be examined in future work.

In this Letter, we have not provided any detailed study of individual structures. Not surprisingly, many regions that show strong, transient substructure have already been the subject of analysis, including loops (Cirtain et al. 2013; Winebarger et al. 2013), dynamics in the moss (Testa et al. 2013), evolution in the filament (Alexander et al. 2013), and anomalous brightenings (Régnier et al. 2014).

We thank the referee for many important observations and comments. We acknowledge the High-resolution Coronal Imager instrument grant funded by NASA's Low Cost Access to Space program. MSFC/NASA led the mission, and partners include the Smithsonian Astrophysical Observatory in Cambridge, MA; Lockheed Martin's Solar Astrophysical Laboratory in Palo Alto, Calif.; the University of Central Lancashire in Lancashire, England; and the Lebedev Physical Institute of the Russian Academy of Sciences in Moscow.

REFERENCES

Alexander, C. E., Walsh, Robert W., Régnier, S., et al. 2013, ApJL, 775, L32
Brooks, D. H., Warren, H. P., Ugarte-Urra, I., & Winebarger, A. R. 2013, ApJL, 772, L19
Cirtain, J. W., Golub, L., Winebarger, A. R., et al. 2013, Natur, 493, 501
Kobayashi, K., Cirtain, J., Winebarger, A. R., et al. 2013, SoPh, in press
Lemen, J. R., Title, A. M., Akin, D. J., et al. 2012, SoPh, 275, 17
Morton, R. J., & McLaughlin, J. A. 2013, A&A, 553, L10
Peter, H., Bingert, S., Klimchuk, J. A., et al. 2013, A&A, 556, A104
Régnier, S., Alexander, C. E., Walsh, R. W., et al. 2014, ApJ, 784, 134
Testa, P., De Pontieu, B., Martínez-Sykora, J., et al. 2013, ApJL, 770, L1
Winebarger, A. R., Walsh, R. W., Moore, R., et al. 2013, ApJ, 771, 21